APPENDIX 3:

ON SOME POSSIBLE INTERACTIONS BETWEEN INTERNAL WAVES AND SEA ICE IN THE MARGINAL ICE ZONE

by

Robin D. Muench and Lon E. Hachmeister

Science Applications, Inc.

and

Paul H. LeBlond

Department of Oceanography
University of British Columbia

March 1982

TABLE OF CONTENTS

LIST OF FIGURES

ABSTRACT

The ice edges of the world ocean are generally the site, at times when winds are blowing off the ice, of regularly-spaced surface bands of ice floes. These bands have size scales of order 1-10 km, and their long axes are oriented approximately normal to the wind direction. Available oceanic temperature and salinity data from the Bering and Greenland Sea ice edge regions suggest that these ice bands are commonly underlain by a two-layered density structure which is maintained by net melting along the ice edges. Linear internal wave theory is applied to these data to compute first-mode interracial wave phase speeds. A simple analytical model is developed which demonstrates the feasibility of generation of such interracial internal waves by the stress discontinuity due to off-ice winds blowing over either a stationary or a moving ice edge. It is qualitatively shown that the computed internal wave phase speeds and wavelengths are, under many conditions, compatible with the speeds and spacings of the surface ice bands. This compatibility suggests, in turn, that coupling between internal waves and ice bands may commonly occur, Some possible implications of the generation and presence of these internal waves upon other ice edge processes, such as air-sea heat and momentum transfer, are qualitatively discussed.

1. INTRODUCTION

The ice-covered regions of the world ocean provide a surface tracer which both responds to and exerts an influence over the underlying water motion. This tracer, floating sea ice, is active rather than passive because it affects the local air-sea heat and momentum transfers as well as responding to them. These interactions are most pronounced along an ice edge where the ice cover is unbounded to seaward and has considerable freedom to respond to and interact with the local water motions.

This paper discusses possible interactions between interracial oceanic internal waves and the floating ice “bands” or “streamers” along an ice edge. Additionally, a new hypothesis is advanced for a mechanism for internal wave generation along an ice edge. The internal wave interactions contribute to explaining the initial divergence of ice near the edge prior to its formation into bands and are consistent with the observed features of the bands and of the regional oceanography.

Section 2 below describes the nature of the ice edge bands and the background oceanic density distribution which has been observed to be associated with ice edges. Section 3 presents a theoretical development of some possible interactions between ice and water, including a mechanism for generation of internal waves by wind action over an ice-water interface. Section 4 discusses the degree to which the theoretical model is consistent with the field observations, and also points out some possible implications of the results with respect to overall air-ice-water interactions along an ice edge.

2. BACKGROUND

With the advent of remote sensing techniques and increased scientific and practical interest in the ice edge regions, a variety of mesoscale and small-scale features have been identified along the ice edges. Of these features, the regularly spaced ice "bands" or "streamers" which occur during off-ice local wind events appear to be universal in occurrence. These features have been documented and studied in the Bering Sea along the winter ice edge [Muench and Charnell, 1977; Bauer and Martin, 19801. They have been documented along the East Greenland Sea ice edge [Wadhams, 19811 and are mentioned by LeBlond [19821 as being evident on satellite imagery of the Labrador Sea winter ice edge. Finally, they have been identified on unpublished satellite images of the Weddell Sea ice edge.

Descriptions of Ice Bands

Descriptions of the ice bands will focus primarily upon those observed in the Bering Sea along the winter ice edge, because the observations from that region are far more complete than those from other regions. A location chart for the Bering Sea shows the location from which data presented here were obtained (Figure 1).

Using satellite imagery, statistics on ice-band spacing for the winter 1974-75 period were compiled by Muench and Charnell 119771. Examination of satellite imagery for the period between 1975 and the present time has suggested that their observations are valid over the longer time period. They observed a mean band spacing of 8.7 km, with a standard deviation of 1.6 km and a variation between 6 and 12 km. These bands were observed to be roughly normal to the wind direction. Their general appearance is shown on Figure 2.

Shipboard observations obtained more recently than Muench and Charnell's work have revealed bands more closely-spaced along the ice edge than were visible on the satellite images. Resolution of these bands, spaced about 1 km apart,

by the satellite was impossible because of the relatively coarse (1 km) resolution of the satellite imagery used. Bauer and Martin 119801, Hachmeister and Muench [1981], Martin and Kauffman [1981] and Martin [this volume] have all reported the widespread presence, during off-ice winds, of these bands spaced about 1 km apart and oriented with their long axes approximately normal to the wind direction. An example of this band configuration obtained from shipboard in March 1981 and reported on by Hachmeister and Muench [1981] is shown in Figure 3. During the transect which yielded the ice distribution shown on Figure 3, the wind was off-ice and steady at about 6 m/see. The computed mean downwind extent of the open water areas between ice bands was 1 km, and the standard deviation was O.5 km; mean width of the ice bands was 0.5 km and the standard deviation was 0.3 km.

Translation speeds for the ice bands are harder to estimate because adequate time-series information is not available. Because of the impossibility of tracking the 10-km spaced bands from day to day using satellite imagery, no estimates of these relatively widely-spaced band speeds are available. Speeds of the more closely-spaced bands which were observed from shipboard varied widely IMartin and Kauffman, 1981; Martin, this volume]. At the start of an off-ice wind event, ice speed was near zero at the time when the bands were first separated from the main body of the ice. Speeds then passed through a wide range, with speeds as high as about 70 cm/sec being observed through use of radar-tracked buoys deployed in specific bands to study their motions. In the absence of more rigorous data, speeds of 20-30 cm/sec are considered typical translation speeds for the bands. Band motion was always in the downwind (seaward) direction, and band formation has never been observed during periods of on-ice wind.

Oceanic Parameters Associated with Ice Edges

Ice edge regions are typically areas of melting. This has been documented, based upon ice distribution and motion, for the Bering Sea by Muench and Ahlnäs [1976] and Pease [1980]. This observation has been supported more recently by oceanic temperature and salinity data [Muench and Pease, 1981; Muench, this volume]. Wadhams [1981] has characterized the East Greenland Sea ice edge as a region of ice melting. A. Gordon [personal communication, 19811 has characterized the Weddell Sea ice edge also as a region of net melting.

A primary effect of ice melting along the edge is to create a strongly two-layered salinity -- hence, density -- structure. The vertical distribution of density underlying the Bering Sea ice edge region in February-March 1981, about mid-winter or during the time of maximum southward ice extent reflects this and is shown on Figure 4. The location of this density transect coincides approximately with that of the ice-band transect illustrated on Figure 3; hence, the density distribution shown was that which underlies the banded structure. Density differences of 0.01-0.3 sigma-t units over a 10-20 m layer were typical, and the interface depth varied from about 30 to 60 m, The two-layered density strut. ture appears to be a regular winter oceanic feature associated with the Bering Sea winter ice edge [Muench and Pease, 1981; Muench, this volume], A set of ver. tical density profiles, obtained at different times from a single location along the Bering Sea ice edge in February-March 1981, illustrates a range of stratifications which appears to be typical for the region (Figure 5).

Vertical density stratification in the Greenland Sea ice edge region is ' greater, at least during summer, than in the Bering Sea. A vertical profile of density in the Greenland Sea ice edge region during summer is shown on Figure 6. The interface between upper and lower layers is extremely strong and sharp.

A second basic difference between the Bering and Greenland Sea ice edge regions, in addition to the degree of stratification, is that between the characteristic bottom depths. Depths underlying the Bering Sea ice edge are typically 80-110 m. Beneath the Greenland Sea ice edge, on the other hand, the bottom falls on the continental slope so that depths vary from 500 to 1000 m and more to seaward.

3. PROPOSED MECHANISM FOR BAND FORMATION AND MAINTENANCE

The mechanisms which form and maintain the ice edge bands are not well understood. Muench and Charnell 11977] hypothesized, based upon analyses of satellite imagery of the Bering Sea winter ice edge, that the larger-scale (lO-km wide) bands were due to interactions between sea ice at the edge and the atmospheric roll vortices which are ubiquitous along the edge during off-ice wind conditions [Walter, 1980]. Bauer and Martin [1980] used results from a 1979 mid-winter field program along the Bering Sea ice edge to hypothesize that band formation was due to a combination of wind stress acting differentially upon the rougher ice along the edge so that a line of ice divergence formed along the edge parallel to it, and radiation stress (due to surface water waves generated in the leads between the bands) which would tend to accelerate the bands away from the main ice pack. Overland and Pease [this volume] present additional evidence that the initial divergence of ice along the edge may be due to wind drag, with accentuation of the divergence through a "sea-breeze" effect. Further arguments in favor of radiation stress as a causative mechanism for the divergence are presented by Wadhams [this volume]. Finally, Hachmeister and Muench [1981] hypothesized, based upon laboratory model results and field data, that the ice" edge bands coincide with surface convergence which are associated with interfacial internal waves beneath the ice edge. They maintained, in addition, that formation of the interracial waves is due either to interaction of ice keels (in regions where the ice is thick enough to have a ridged structure) with the oceanic stratification or to response of the stratified ocean to a nonuniform wind stress where the nonuniformity is due to the surface presence of the ice edge,

Of the mechanisms for ice band formation listed above, only that involving interaction with internal waves provides a satisfactory explanation for the observed regular spacing of the bands. This paper explores some possible interactions

between ice edge bands and oceanic internal waves in more detail, with the intention of clarifying the dynamic processes involved and demonstrating compatibility between the observed ice features and internal waves.

The development presented here follows two avenues of approach. First, linearized theory is used to estimate ranges for the first-mode interracial internal-wave phase speeds appropriate to the density differences observed in the Bering and Greenland sea ice edge regions. Second, an analytical solution is derived for the generation of internal waves by a wind stress acting across the surface discontinuity presented by an ice edge.

Estimation of Representative Interracial Wave Phase Speeds

In the simplest physical sense, the oceanic regimes underlying the Bering and Greenland Sea ice edges may be considered as two-layered systems separated by a horizontal density interface. In order to establish ranges for parameters to be used in the following analytical development, and also as a prelude to establishing compatibility between internal wave and ice band parameters it is useful to compute representative values of interracial internal-wave phase speeds which might be expected given the oceanic conditions observed in association with ice edges. The upper- and lower-layer densities, interface depth, and bottom depths used in the computations include the ranges which we would expect, based upon available data, to occur in the Bering or Greenland Sea ice edge regions (see, for example, Figures 4-6).

The computations used for arriving at the first-mode interracial wave speeds are based upon a two-layered fluid model given in Turner 119731. The basic equation for the phase speed c is

$$c^2 = \frac{g\Delta\rho}{k}(\rho_1 \coth kh_1 + \rho_2 \coth kh_2)^{-1} \qquad (1)$$

where h_1 = upper layer thickness, h_2 = lower layer thickness, ρ_1 = upper layer density, P_2 = lower layer density, and Ap = density difference between layers. In the shallow-water long-wave case appropriate to the Bering Sea ice edge region, kh_1 and kh_2 both approach zero and Equation (1) can be approximated by

$$c^2 = \frac{g\Delta\rho}{\rho_2} \frac{h_1 h_2}{(h_1 + h_2)} .$$

For waves which are at least as long as the lower layer depth, this approximation is also appropriate to the Greenland Sea ice edge region; now, since $h_2 >> h_1$, Equation (1) becomes, for the Greenland Sea,

$$C^2 = \frac{g\Delta\rho}{\rho_2} h_1 .$$

Table 1 gives the computed values for c using varying upper layer thicknesses and density differences between the layers.

The above computations assumed small-amplitude waves, allowing use of linear theory. Even if the waves were of large enough amplitude to violate this assumption, the results would not be greatly different. Holyer 11979] has demonstrated, using theoretical arguments, that at the largest amplitudes the phase speeds of long waves are only about 20% higher than those for infinitesimal waves, Given the approximate nature of the estimated band speeds presented above, a 20% error in computed wave phase speeds would not substantially alter the conclusions which are presented below.

A Mechanism for Wind-Generation of Internal Waves

A theoretical development is presented here of a mechanism for generation at an ice edge of internal waves by the nonuniform wind stress due to off-ice winds. This proposed mechanism is schematically illustrated on Figure 7. It is

assumed, in concert with observations, that the wind is blowing in the off-ice direction and that the ice edge is underlain by an oceanic structure two-layered in density. Location "A" on Figure 7 indicates the region where divergence in the ice cover first occurs. In a region referred to on the figure as the "generation" region, the wind blowing off-ice either across a band or off the main mass of ice causes a localized upwelling tendency due to surface divergence. This is illustrated by the upward-bulging of the interface in the middle of the generation region. This bulge will then propagate in both directions, as shown, as trains of interracial waves. Point "B" signifies the boundary between the generation region and the propagation region through which the ensuing internal wave train moves. Those waves traveling in the off-ice direction at phase speed c will tend to collect floating ice in the convergence overlying the wave troughs, as shown. Waves traveling in the opposite direction, beneath the ice edge, might contribute to surface divergence of the ice pack there.

Internal wave generation at the seaward edge of a moving ice cover may be analyzed in a simple model. The vertical density distribution is approximated in terms of a two-layered structure with linear phase speed c as estimated above. With x measured positively from the uniformly moving (at speed V) ice edge and y along it, two-dimensional ($\partial_y = 0$) perturbations of the stratified fluid from its equilibrium state are governed by the long-wave equations

$$\frac{\partial u_1}{\partial t} - V \frac{\partial u_1}{\partial x} - f v_1 = -g \frac{\partial \eta}{\partial x} + \frac{\tau}{\rho_1 h_1} \qquad (2a)$$

$$\frac{\partial v_1}{\partial t} - V \frac{\partial u_1}{\partial x} + f u_1 = 0 \qquad (2b)$$

$$h_1 \frac{\partial u_1}{\partial x} = -\left(\frac{\partial}{\partial t} - V \frac{\partial}{\partial x}\right)(\eta - \zeta) \simeq \left(\frac{\partial}{\partial t} - V \frac{\partial}{\partial x}\right)\zeta \qquad (2c)$$

$$\frac{\partial u_2}{\partial t} - V\frac{\partial u_2}{\partial x} - fv_2 = -g\frac{\rho_1}{\rho_2}\frac{\partial \eta}{\partial x} - g\frac{\Delta\rho}{\rho_2}\frac{\partial \zeta}{\partial x} \qquad (3a)$$

$$\frac{\partial u_2}{\partial t} - V\frac{\partial u_2}{\partial x} + fu_2 = 0 \qquad (3b)$$

$$h_2\frac{\partial u_2}{\partial x} = -\left(\frac{\partial}{\partial t} - V\frac{\partial}{\partial x}\right)\zeta \ . \qquad (3c)$$

Subscripts 1 and 2 refer to the upper and lower layers, respectively. The surface displacement η is assumed of order $\zeta\Delta\rho/\rho_2$ and neglected, as appropriate for internal waves. The stress τ changes value at the ice edge (x=0). For $x < 0$, the surface stress is applied to the water as $\tau = \rho_1 c_w (V-u_1)^2$ with C_w the ice-water drag coefficient; for $x > 0$, the wind stress is exerted directly on the water surface, i.e. $\tau = \rho_{air} c_D (U-u_1)^2$, with CD the air-water drag coefficient and U the wind speed. This discontinuity in stress generates the internal waves.

Eliminating all variables but ζ from (2) and (3), we find

$$\zeta_{tt} - 2V\zeta_{xt} - (C^2 - V^2)\zeta_{xx} + f^2\zeta = -\frac{C^2}{\rho_1 h_1}\tau_x \ , \qquad (4)$$

where c is the long-wave speed, i.e. $C^2 = g(\Delta\rho/\rho_2)[h_1h_2/(h_1+h_2)]$. Free-plane wave solutions of the homogeneous form of Equation (4) are shortened when they travel against V, i.e. in the +x direction, and lengthened when they travel under the ice away from the edge in the -x direction. Near resonance ($V \simeq c$) the wavelength ahead of the ice becomes

$$\lambda \simeq \frac{\pi c}{\omega}\left(1 - \frac{V^2}{c^2}\right) \ . \qquad (5)$$

Measured seaward ice speeds V are comparable to the calculated internal wave speeds c, so that even for rather long-period forcing ($T = 2\pi/\omega \sim 1$ day, as for sea-breeze winds, for example) λ can approach the observed ice band spacing near resonance. The alternation on a scale λ of surface flow divergence and convergence, as given by $\partial u_1/\partial_x$, would then contribute to the sum of forces (wind, waves) which determine ice band spacing.

As a more specific extension of the above case, we may consider the forced initial value case wherein internal waves are produced from rest by a wind stress of the form

$$\tau = F(t)[\tau_o + A_\tau H(x)] \quad , \tag{6}$$

where H(x) is the Heaviside step function, $\Delta\tau$ is the stress discontinuity across x = 0, and F(t) describes the time-dependence of the stress with F(0) = 0. Taking the Laplace transform of Equation (4) ($\partial_t \to p$) and applying the matching conditions

$$\lim_{x\to 0} \bar{\zeta}(x < 0) = \lim_{x\to 0} \bar{\zeta}(x > 0) \tag{7a}$$

$$\left(1 - \frac{V^2}{c^2}\right)\left[\lim_{x\to 0} \bar{\zeta}_x\ (x > 0) - \lim_{x\to 0} \bar{\zeta}_x\ (x < 0,\right] = -\frac{\bar{F}(P)\Delta\tau}{\rho_1 h_1} \tag{7b}$$

across x = o on the transformed variables (denoted by overbars), we find that

$$\bar{\zeta}_+(x,P) = \frac{c\Delta\tau\ \bar{F}(P)}{2\rho_1 h_1\left[P^2 + \left(1 - \frac{V^2}{c^2}\right) f^2\right]^{1/2}} \exp\left\{\frac{-VPx}{(c^2 - v^2)} - \left[P^2 + \left(1 - \frac{V^2}{c^2}\right)f^2\right]^{1/2}\frac{|x|}{c}\right\}. \tag{8}$$

The surface layer divergence is obtained from (2c) as

$$h_1\bar{u}_{1_X} = \frac{CAT\ \bar{F}(P)}{2\rho_1 h_1} \left(\frac{c^2 P/(c^2 - V^2)}{\left[P^2 + (1 - \frac{V^2}{c^2}) f^2 \right]^{1/2}} \pm \frac{V}{c} \right) \exp\left\{ \ldots \right\} \quad \text{“ ‘g)}$$

The argument of the exponential in Equation (9) is the same as in Equation (8) and is not repeated. Near resonance, V → c and the first term in Equation (9) will dominate for $P^2/(1 - \frac{V^2}{c^2})f^2 \simeq o(1)$. For a step-function wind stress, $\bar{F}(P) = 1/P$, and a tabulated inverse is found for $h_1\bar{u}_{1_X}$ [Abramowitz and Stegun, 1965, Ch. 291,

$$h_1 u_{1_x}(x,t) = \frac{c\Delta\tau}{2\rho_1 h_1 (1 - \frac{V^2}{c^2})} J_o\left((1 - \frac{V^2}{c^2})^{1/2} f \sqrt{\left(t - \frac{|x|V}{c^2 - V^2} \right)^2 - \frac{x^2}{c^2}} \right) H\left(t - \frac{|x|V}{(c^2 V^2)} - \frac{|x|}{c} \right) \quad (10)$$

As we would expect, the response becomes singular at resonance, i.e. as soon as the ice field velocity approaches the internal wave speed, a strong pattern of surface divergence is set up with spatial dependence given by Equation (10) for an impulsive wind stress or by the convolution of Equation (10) with the appropriate transform for a different stress history. The position of the first zero of the Bessel function gives an estimate of the scale from the ice edge to the first zone of maximum divergence (or convergence, depending on the sign of AT). For $x > 0$, this first zero occurs at

$$\left(t - \frac{xV}{c^2 - V^2} \right)^2 = \frac{3.8}{f^2 (1 - \frac{V^2}{c^2})} + \frac{x^2}{c^2} . \quad (11)$$

The scale length of the Bessel function decreases as its argument, which is roughly proportional to t, increases. We then seek to know, using Equation (11),

whether a scale $x \sim 10^3$ m which is of the order of the observed band spacing can arise in a reasonable value of the time elapsed since the wind began to blow. With $x \simeq 10^3$ m, $c \simeq 50$ cm/see, and $V \simeq 0.9\ c$, then $t \simeq 5 \times 10^4$ sec $\simeq 0.5$ day, which is short enough to respond to a diurnal sea-breeze type of forcing.

4. DISCUSSION

The field data available from the Bering and Greenland Sea ice edge regions have been obtained for use primarily in analyses of mesoscale processes. Consequently, the spatial and temporal resolutions of these data make them inadequate to rigorously determine whether internal wave mechanisms such as discussed above (Section 3) are in fact significant in those regions. Nevertheless, reference to the computed first-mode internal wave speeds c presented in Table 1 reveals that ice speeds of up to about 35 cm/sec would be compatible with the internal wave phase speeds computed using the stratification observed along the Bering Sea ice edge. Computed first-mode internal wave speeds for the Greenland Sea ice edge are higher than those for the Bering (Table 1). We therefore expect that interracial waves along the Greenland Sea ice edge would have a much greater range of propagation speeds than in the Bering. While no data are available on ice band motion along the Greenland Sea ice edge, it seems reasonable that the speeds of these bands would tend to fall within the range of possible speeds shown in Table 1 and that their interaction with internal waves would be consistent with physical reasoning. This supposition is supported by the consistency between computed internal wavelength λ and observed ice band spacing.

A single time series of current and temperature, obtained from the Bering Sea winter ice edge region, revealed oceanic features which are consistent with the presence of internal waves. This record was obtained at 50-m depth and was sampled at 30-minute intervals (Figure 8). During the January-February 1981 period, the interface between the upper and lower oceanic layers beneath the ice edge (see Figure 4) moved toward the south-southwest past this mooring as the ice cover advanced toward its annual maximum southward extent. Temperature variations coincide with density variations because the upper lower-density layer is colder than the denser lower layer [Muench, this volume] , The temperature

record from the mooring revealed rapid (i.e. of the same order as or having shorter period than the 30-minute sampling intervals of the instruments) temperature fluctuations while the density/temperature interface was passing by the current meters (Figure 8). Current speed fluctuations were present at the same time. The maximum recorded temperatures, which occurred early in the portion of the record shown and were about +1.3 °C, were those in the warmer lower layer of water. The minimum temperature (-1.7 “C), which occurred later in the record segment shown on Figure 8, was typical of the colder upper-layer water. The lower- and upper-layer water temperatures therefore provided an “envelope” of maximum and minimum temperatures, Presence of the fluctuations between these maximum and minimum values, superposed upon the overall trend toward lower temperature as the current meter was surrounded by the colder upper-layer water, suggest that vertical oscillations of the interface between the upper and lower layers were occurring. These oscillations were sufficient to vertically move the entire temperature gradient region past the current meter. Reference to the profiles shown on Figure 5 suggests that vertical oscillations of 10-20 m amplitude would have been necessary to achieve this.

High-frequency oscillations in current speed were also present. They were superposed upon a tidal current signal and were less obvious than the corresponding temperature oscillations. Because of the relatively widely-spaced sampling interval (30 minutes), it was not possible to examine phase relations between the current and temperature fluctuations in the frequency range of interest. Visual inspection of the current fluctuations shown on Figure 8 suggests that peak associated speeds were about 5 cm/sec.

Although these data are clearly inadequate for a rigorous analysis, they nevertheless demonstrate that -vertical notions of the interface between layers were present and had time scales of about 30 minutes, Such time scales would be consistent with interracial waves phase-locked with surface ice bands.

In addition to providing a physically satisfying explanation for one of the more widespread medium-scale ice edge features, the results presented above can be expected to have significant consequences for other ice-edge processes. A major factor would be the additional "form drag" term due to interaction of the ice bands with the internal waves. This term must be considered when using observed winds, ice speeds, and oceanic currents to compute the air-sea-ice momentum transfer. Sea ice moves across the ocean surface under the influence of both internal stresses in the ice and coupling with the wind and upper layers of the ocean. Coupling between ice and ocean affects both ice motion and the dynamics of the upper ocean layer, and more than one such coupling mechanism exists between the ice and ocean. In the absence of oceanic stratification, drag forces between the ice and the water result from a combination of skin friction (applied over the entire underside of the ice) and form drag exerted by irregularities on the lower side of the ice cover. In a stratified fluid an additional coupling mechanism exists: as demonstrated by Ekman 119061, internal waves generated by a large obstacle can contribute a significant wave resistance to the total drag on an obstacle moving in a stratified fluid, Hachmeister and Rigby [19801 modeled this mechanism in a laboratory tow tank and detected drag increases of nearly 150% due to the internal wave-sea ice coupling. The internal wave/ice band interactions suggested here would tend to limit the off-ice translation speed of ice bands to the internal-wave phase speed. Since the rate of ice melting at the edge is dependent to some extent on the ambient water temperature, and the water temperature increases away from the ice edge, the speed with which the bands move into warmer water is critical to estimation of melting rates. The results of this investigation therefore impact on both air-sea-ice momentum transfer and the melting rates of ice along the edge.

Finally, the internal waves generated by a stress discontinuity at the ice edge set up surface layer divergence bands behind as well as ahead of the ice edge and contribute to opening up of leads as well as to compacting of ice bands ahead of the ice edge. Of course, as soon as the original ice edge becomes accompanied both fore and aft by other ice edges, the simple conditions of the above analysis no longer prevail. For example, surface wave radiation stress would then tend to compact the ice bands from the rear and accelerate them to seaward. However, the above arguments should be sufficient to demonstrate that coupling between ice bands and internal waves is possible on the scales observed in nature.

Rigorous testing of the hypotheses presented above awaits the acquisition of new field and laboratory data. It is hoped that the current growing interest in marginal ice zone problems will enable such a testing program to be carried out.

5. ACKNOWLEDGEMENTS

The satellite image used in the manuscript was kindly supplied by Dr. Seelye Martin of the University of Washington. This work has been funded by the Office of Arctic Programs, Office of Naval Research, under contract NOO014-82-C-O064 and by the Bureau of Land Management through interagency agreement with the National Oceanic and Atmospheric Administration, under which a multi-year program responding to needs of petroleum development of the Alaskan continental shelf is managed by the Outer Continental Shelf Environmental Assessment Program (OCSEAP) office.

REFERENCES

Abramowitz, M., and I. Stegun, Handbook of Mathematical Functions, Dover, New York, 1965.

Bauer, J., and S. Martin, Field observations of the Bering Sea ice edge properties during March 1979, Mo. Wea. Rev., 108, 2045-20S6, 1980.

Ekman, V.M., On dead-water, in The Norwegian North-Polar Expedition, 1893-96, Scientific Results, Vol. 5 (cd., F. Nansen), Christiana, Norway, 1-152, 1906.

Hachmeister, L.E., and F.A. Rigby, Laboratory studies of stratified flow interaction with topography, Proc. Second IAHR Symp , on Strat. Flows, Vol. II, Trondheim, Norway, 623-635, 1980.

Hachmeister, L.E., and R.D. Muench, Interactions between internal waves and ice bands in the marginal ice zone, Eos, 62, 895, 1981.

Holyer, J.Y., Large amplitude progressive interracial waves, J. Fluid Mech., 93, 433-448, 1979.

LeBlond, P.H., Satellite observations of Labrador Current undulations, Atmos.-Ocean. in press, 1982.

Martin, S., The movement and decay of ice edge bands in the winter Bering Sea, J. Geophys. Res., this volume.

Martin, S., and P. Kauffman, The movement and decay of ice edge bands in the winter Bering Sea, Eos, 62, 895, 1981.

Muench, R.D., Some circulation and hydrographic features associated with the Bering Sea ice edge region, J. Geophys. Res., this volume.

Muench, R.D., and K. Ahlnäs, Ice movement and distribution in the Bering Sea from March to June 1974, J, Geophys. Res., 81, 4467-4476, 1976.

Muench, R.D., and R.L. Charnell, Observations of medium-scale features along the seasonal ice edge in the Bering Sea, J, Phys. Oceanogr. , 7, 602-606, 1977.

Muench, R.D., and C.H. Pease, Mid-winter interactions between a two-layered hydrographic structure and the ice edge on the central Bering Sea shelf, Eos, 62, 890, 1981.

Overland, J.E., and C.H. Pease, Local acceleration of the wind as a mechanism for divergence in the marginal ice zone, J. Geophys. Res., this volume.

Pease, C.H., Eastern Bering Sea ice processes, Mo. Wea. Rev., 108, 2015-2023, 1980.

Turner, J.S., Buoyancy Effects in Fluids, Cambridge Univ. Press, Cambridge, England, 1973.

Wadhams, P., The ice cover in the Greenland and Norwegian seas, Rev. Geophys. and Space Phys., 19, 345-393, 1981,

Wadhams, P., A mechanism for formation of ice edge bands, J. Geophys. Res., this volume.

Walter, B.A., Wintertime observations of roll clouds over the Bering Sea, Mo. Wea. Rev., 108, 2024-2031, 1980.

Table 1. Computed first-mode internal wave speed c in cm/sec for the Bering Sea and Greenland Sea cases. Ap is the density difference in g/cm^3 across the interface between the upper and lower layers; h is the depth of the interface in meters.

CASE	Δρ → / h ↓	0.00010	0,00025	0.00050	0.00100	0.00500
Bering Sea						
(bottom depth ∿ 100 m)	25	14	22	30	42	96
	50	16	26	36	51	114
	75	15	24	34	48	107
E. Greenland Sea						
(bottom depth > 1000 m)	25	15	24	35	49	109
	50	22	35	49	69	155
	75	27	42	60	85	189

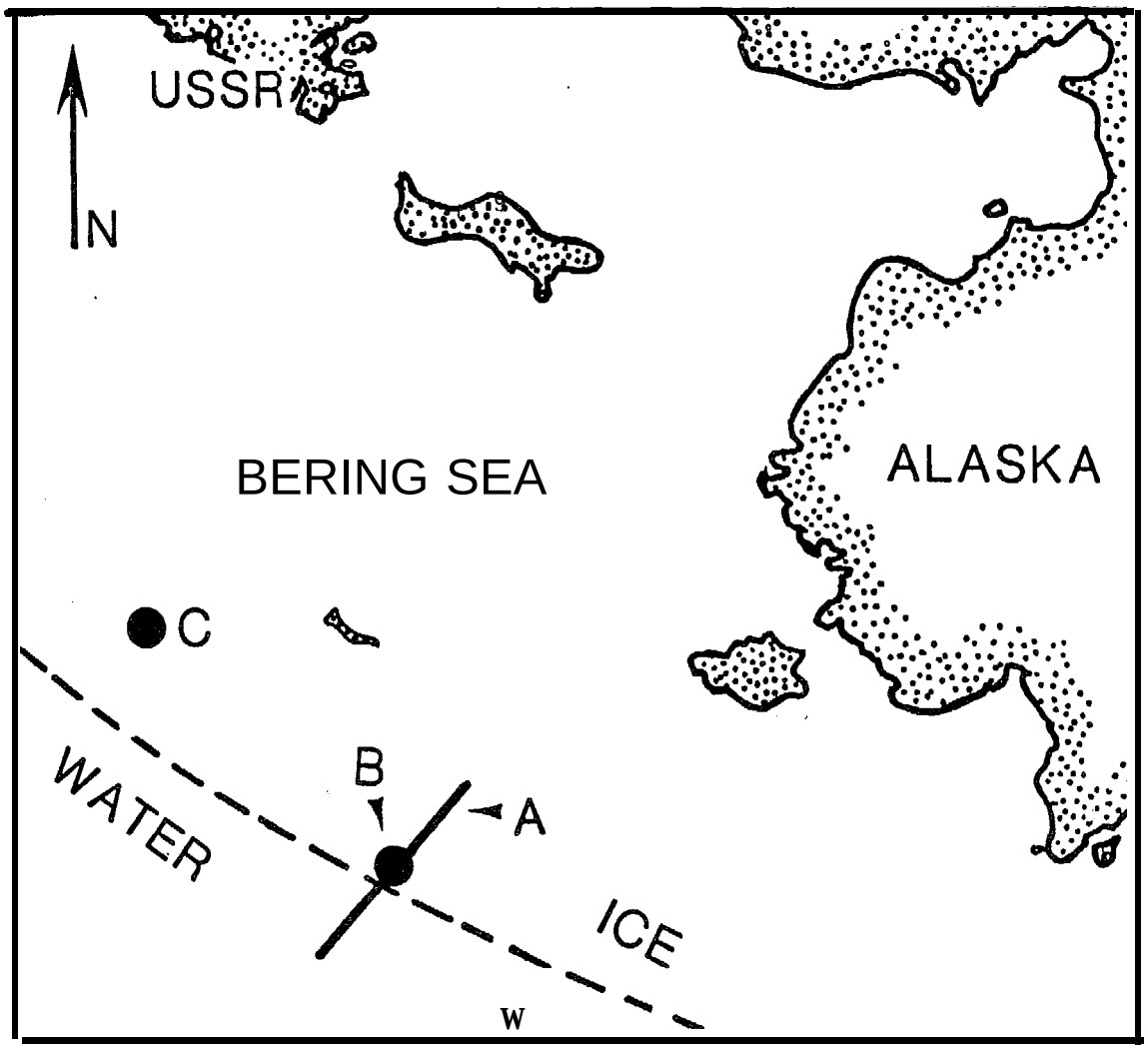

Figure 1. Location figure for data shown which were obtained from the Bering Sea ice edge region. Letter designations “A”, “B” and "C" are explained in the appropriate figure legends.

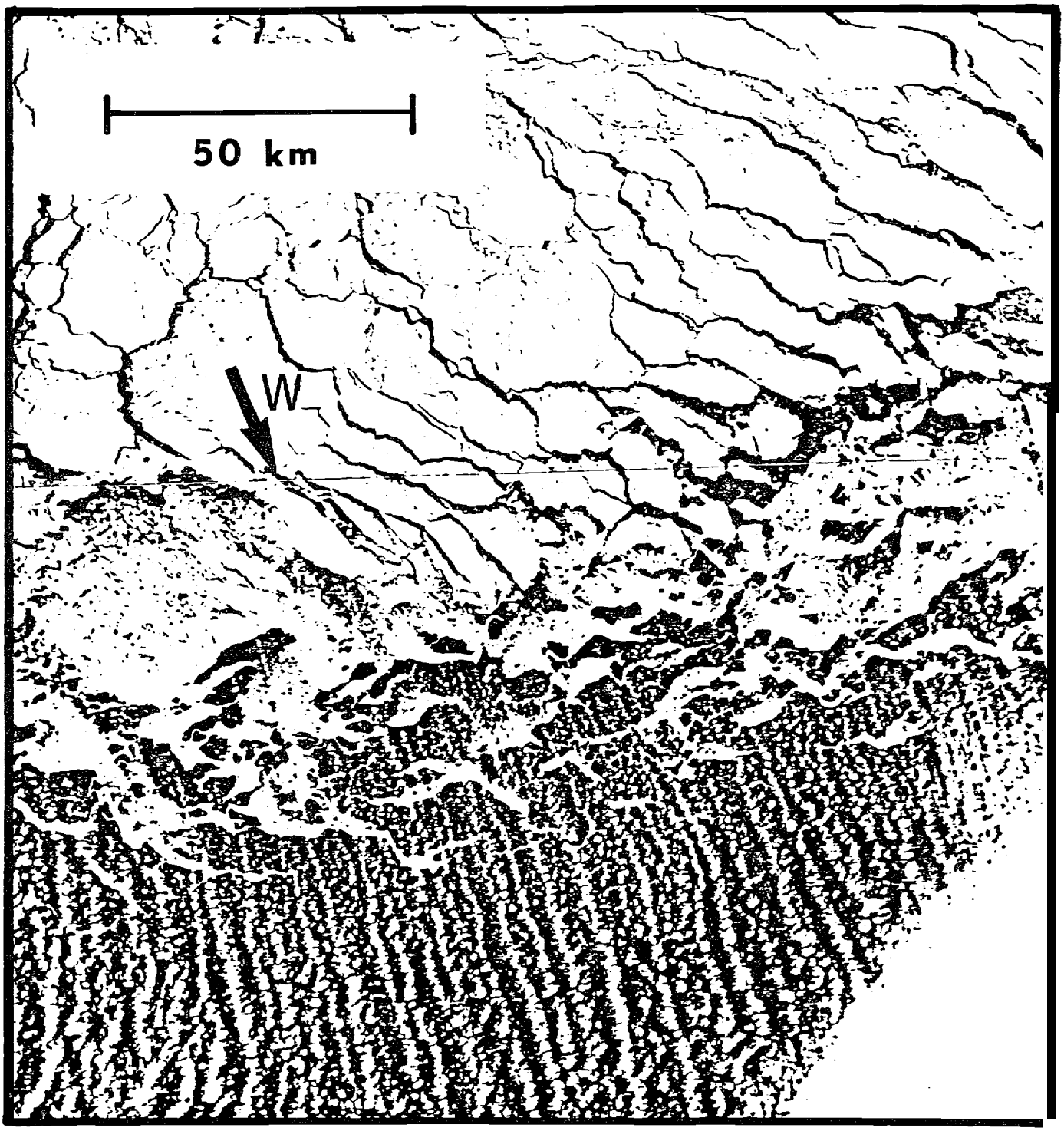

Figure 2. NOAA satellite image showing ice edge bands along the Bering Sea winter ice edge. Arrow "W" indicates approximate wind direction.

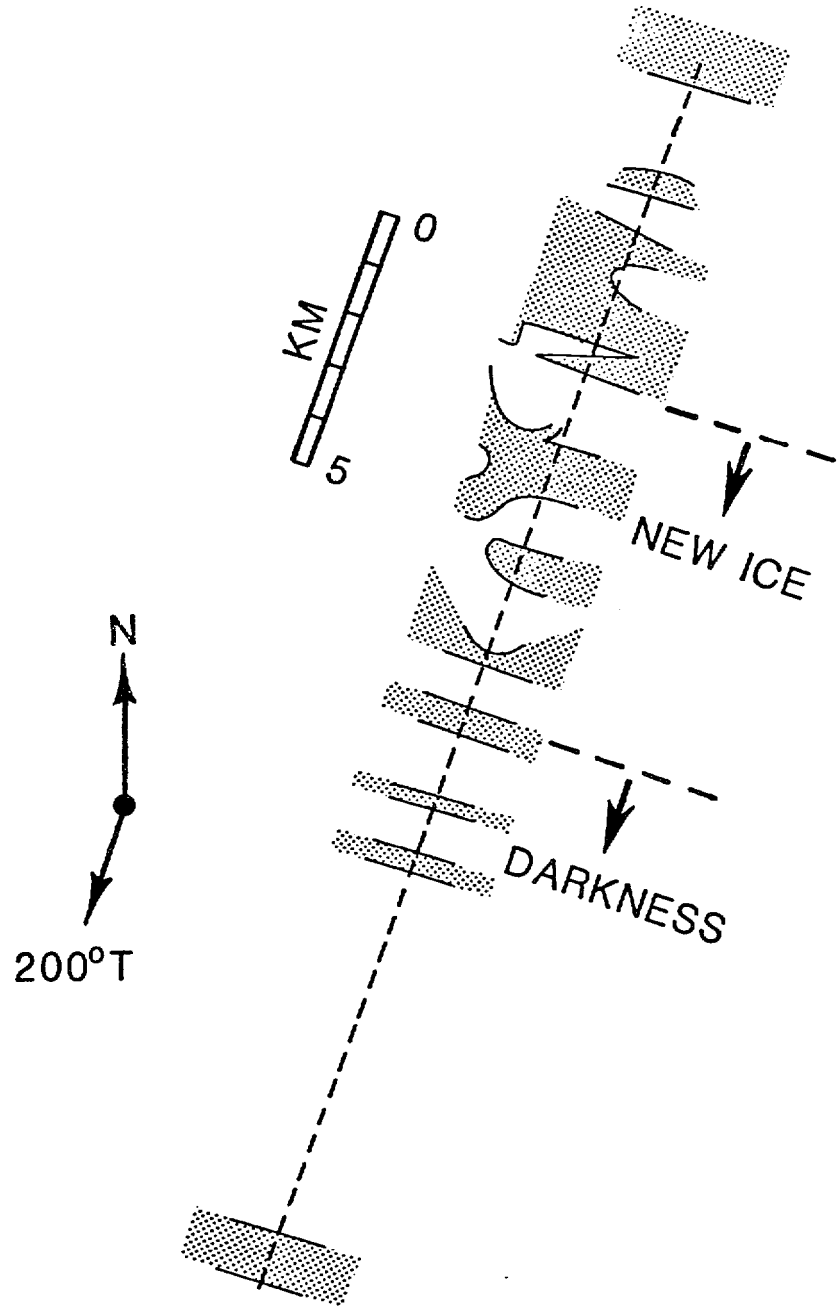

Figure 3. Schematic of ice bands along the Bering Sea ice edge late on 7 March 1981. Observations were obtained from a surface vessel traveling toward zoo “T along the dashed line, South of the border “new ice”, no rafting or ridging was evident and most ice appeared to be only a few days old. After dark it became impossible to discern details of the ice. The wind was steady at about 6 m/see toward 200 ‘T throughout the transect, Approximate location of transect is shown as southern part of line “A” on Figure 1.

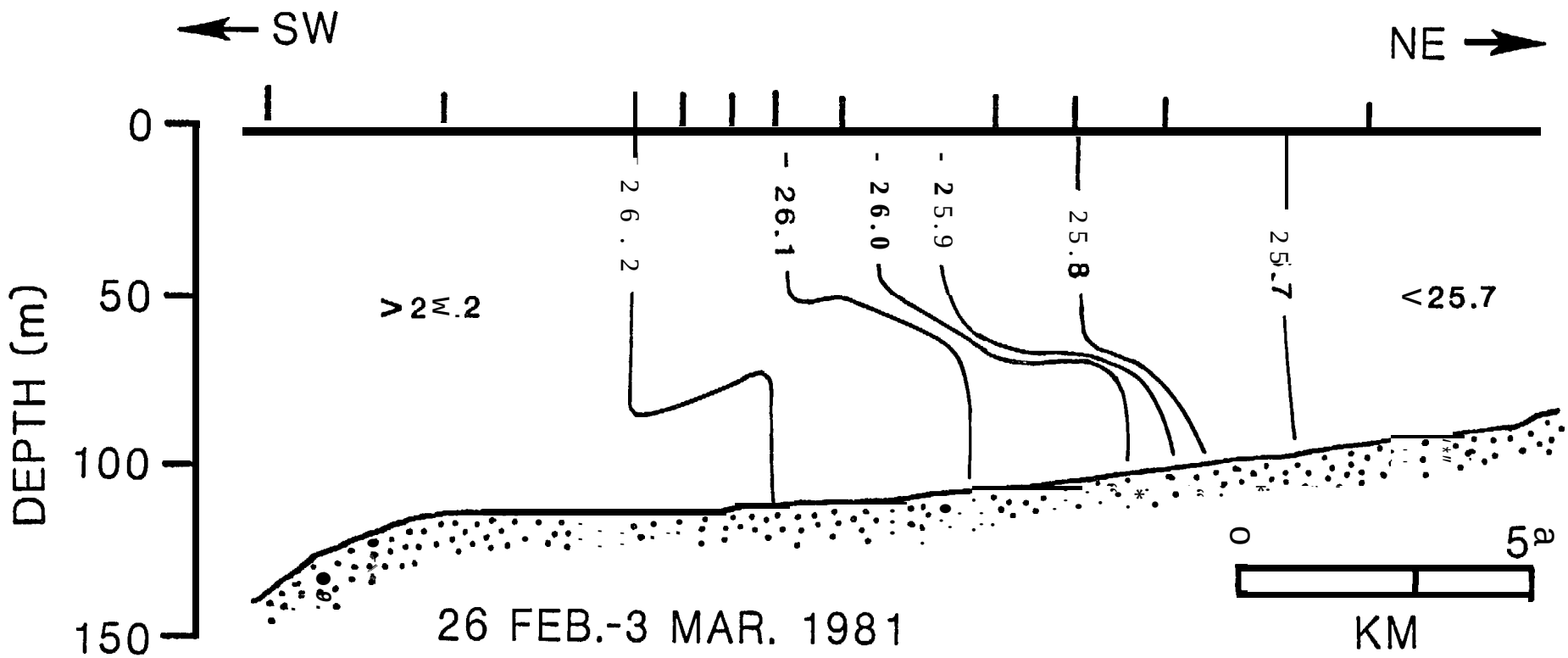

Figure 4. Vertical distribution of density as sigma-t) along a transect across the Bering ice edge in mid-winter 1981. Approximate location of transect is shown as line "A" on Figure 1.

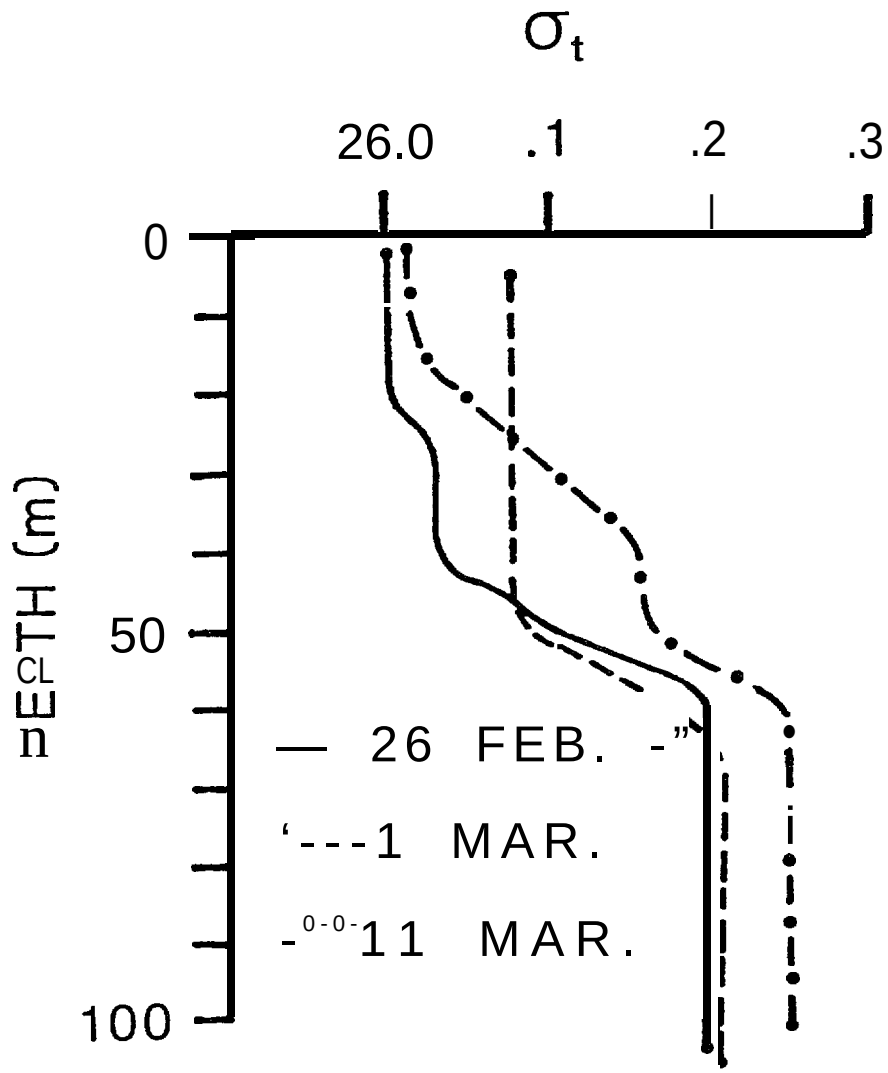

Figure 5. Illustration of variability in vertical density {as sigma-t) distribution at a single position near the Bering Sea ice edge over a 14-day period in mid-winter 1981. Bottom depth was 109 m. Approximate location of station is shown as point "B" on Figure 1,

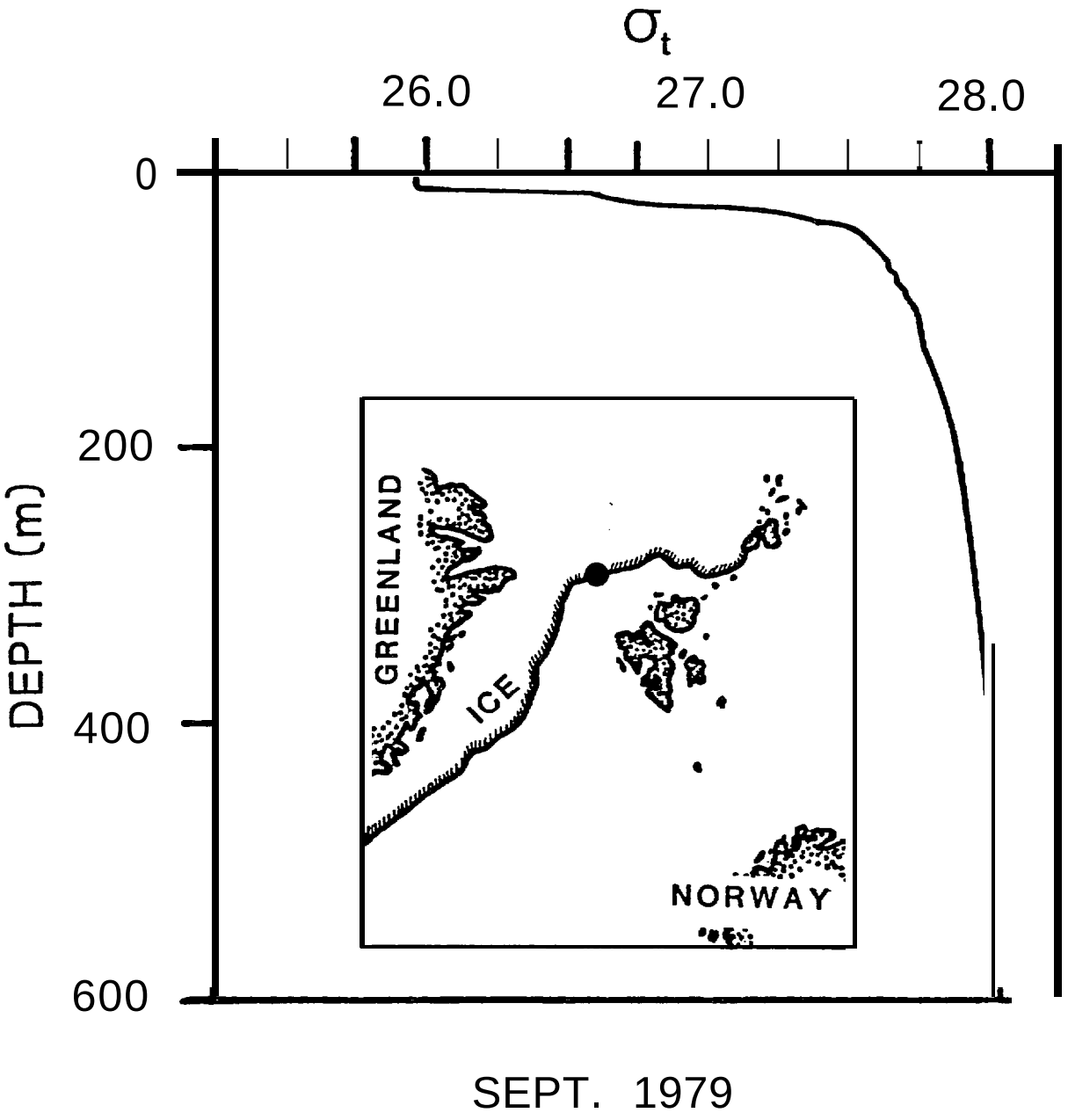

Figure 6. Example of vertical density (as sigma-t) distribution at a location near the Greenland Sea ice edge in late summer 1979. Bottom depth was greater than 700 m. Inset map shows approximate location of station.

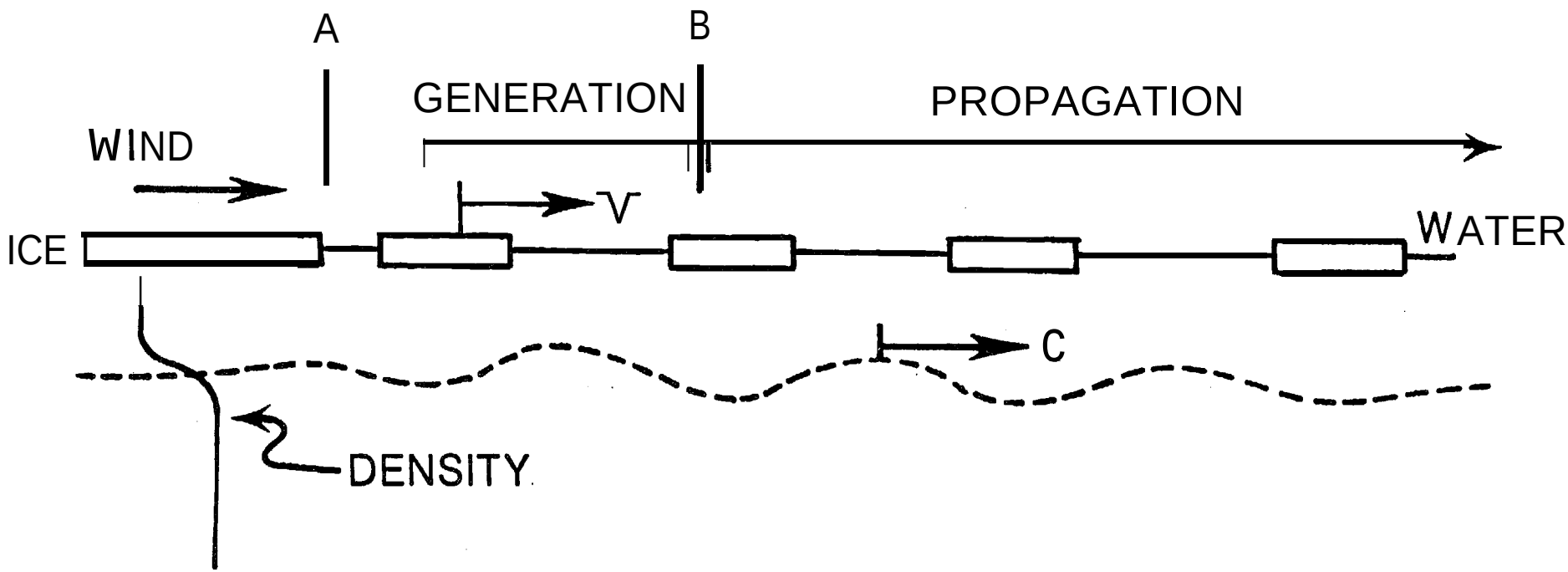

Figure 7. Schematic diagram illustrating the conceptual model discussed in the text.

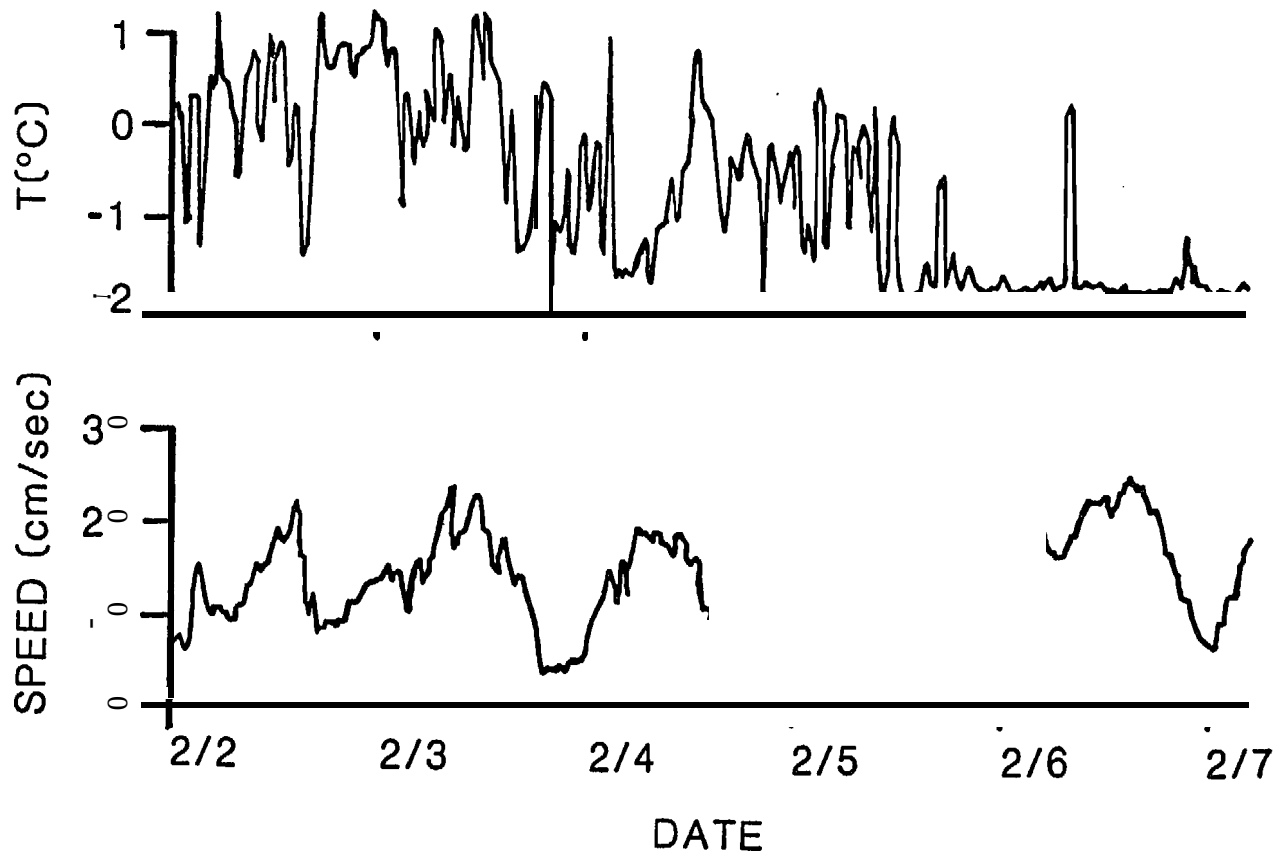

Figure 8. Time-series of temperature (upper) and current speed (lower) obtained in the density interface at 50-m depth below the Bering Sea ice edge in early February 1981. Approximate location of mooring from which data were obtained is shown as point "C" on Figure 1.